Journal of Energy Chemistry 60 (2021) 9–15

Contents lists available at ScienceDirect

Journal of Energy Chemistry

journal homepage: www.elsevier.com/locate/jechem

http://www.journals.elsevier.com/journal-of-energy-chemistry/

Real-time monitoring of the lithiation process in organic electrode 7,7,8,8-tetracyanoquinodimethane by *in situ* EPR

Mingxue Tang [a,b], Nhat N. Bui [b], Jin Zheng [a,b], Likai Song [b], Yan-Yan Hu [a,b,*]

[a] *Department of Chemistry and Biochemistry, Florida State University, Tallahassee, FL 32306, USA*
[b] *National High Magnetic Field Laboratory, 1800 East Paul Dirac Drive, Tallahassee, FL 32310, USA*

ARTICLE INFO

Article history:
Received 11 November 2020
Revised 11 December 2020
Accepted 15 December 2020
Available online 31 December 2020

Keywords:
Organic electrode
In situ EPR
Rechargeable batteries
7,7,8,8-tetracyanoquinodimethane

ABSTRACT

Organic electrodes are advantageous for rechargeable lithium-ion batteries owing to their high theoretical capacities, diverse functionalities, and environmental compatibility. Understanding the working mechanism of organic electrodes is vital to strategic materials design. However, due to lack of suitable characterization tools, it has been challenging to probe the reaction processes of organic electrodes in real-time. Here, non-destructive *in situ* electron paramagnetic resonance (EPR) was performed on a model organic electrode, 7,7,8,8-tetracyanoquinodimethane (TCNQ) used in rechargeable lithium-ion batteries, to directly follow the redox reactions in real-time. In order to minimize interfering signals from other parts of the batteries than the TCNQ electrode of interest, two sets of batteries are fabricated and studied with *in situ* EPR: (1) a $LiCoO_2$//$Li_4Ti_5O_{12}$ full-cell battery to determine the EPR signal evolution of additives and electrolytes; (2) a $LiCoO_2$//TCNQ battery, and the difference in the observed EPR signals reflects purely the redox reactions of TCNQ upon lithiation and delithiation. A two-electron reversible redox reaction is delineated for TCNQ. TCNQ dimers form during the first electron injection upon lithiation and followed by the break-down of the dimers and associated electron coupling to produce massive delocalized electrons, resulting in increased EPR signal during the 2nd electron injection. Reversible trends are observed during electron ejection upon delithiation. *In situ* EPR is very sensitive to electron activities, thus is a powerful tool to follow redox reactions of organic electrodes, allowing for improved fundamental understanding of how organic electrodes work and for informed design of high-performance organic materials for energy storage.

1. Introduction

Electrodes with high energy and high power densities, good stability, low cost, and environmental compatibility are in need for high-performance rechargeable batteries [1–5]. The specific capacities of inorganic electrodes are limited by the redox reactions of transition metal elements and structural rigidity. By contrast, organic electrodes show potential in producing high gravimetric capacity via multi-electron reactions through functionalization. In addition, their sustainability and environmental compatibility are also appealing [6–8]. However, a major challenge for organic electrodes is capacity degradation due to decomposition and or solubility in electrolytes. Polymerization and salt formation are two effective approaches to improve their cycling stability [7,9,10]. Solid-state batteries can circumvent the issue of high solubility in organic solvents [6,11,12]. Very recently, metal–organic framework (MOF) has been proposed as another way to improve the cycling performance together with increased capacity by additional transition metal redox [13,14].

Among all the organic electrodes, quinone-based materials [8,12,15] with cyanide groups show high capacity and good cycling reversibility [16–20]. However, the lithiation and delithiation mechanisms of these materials are elusive and fundamental understanding of how these organic electrodes work in rechargeable batteries in real-time will provide guidelines on how to modify their structures to achieve improved electrochemical performance. 7,7,8,8-tetracyanoquinodimethane (TCNQ) is one of the representative organic electrodes used in rechargeable lithium-ion batteries. Extensive efforts have been directed towards understanding the interactions of Li^+ and e^- within the organic structural framework. Lithiation and delithiation are usually accompanied by changes in electron band structures and charge re-distribution. Some reports claimed that free radicals are formed upon lithiation

* Corresponding author.
E-mail address: yhu@fsu.edu (Y.-Y. Hu).

https://doi.org/10.1016/j.jechem.2020.12.009

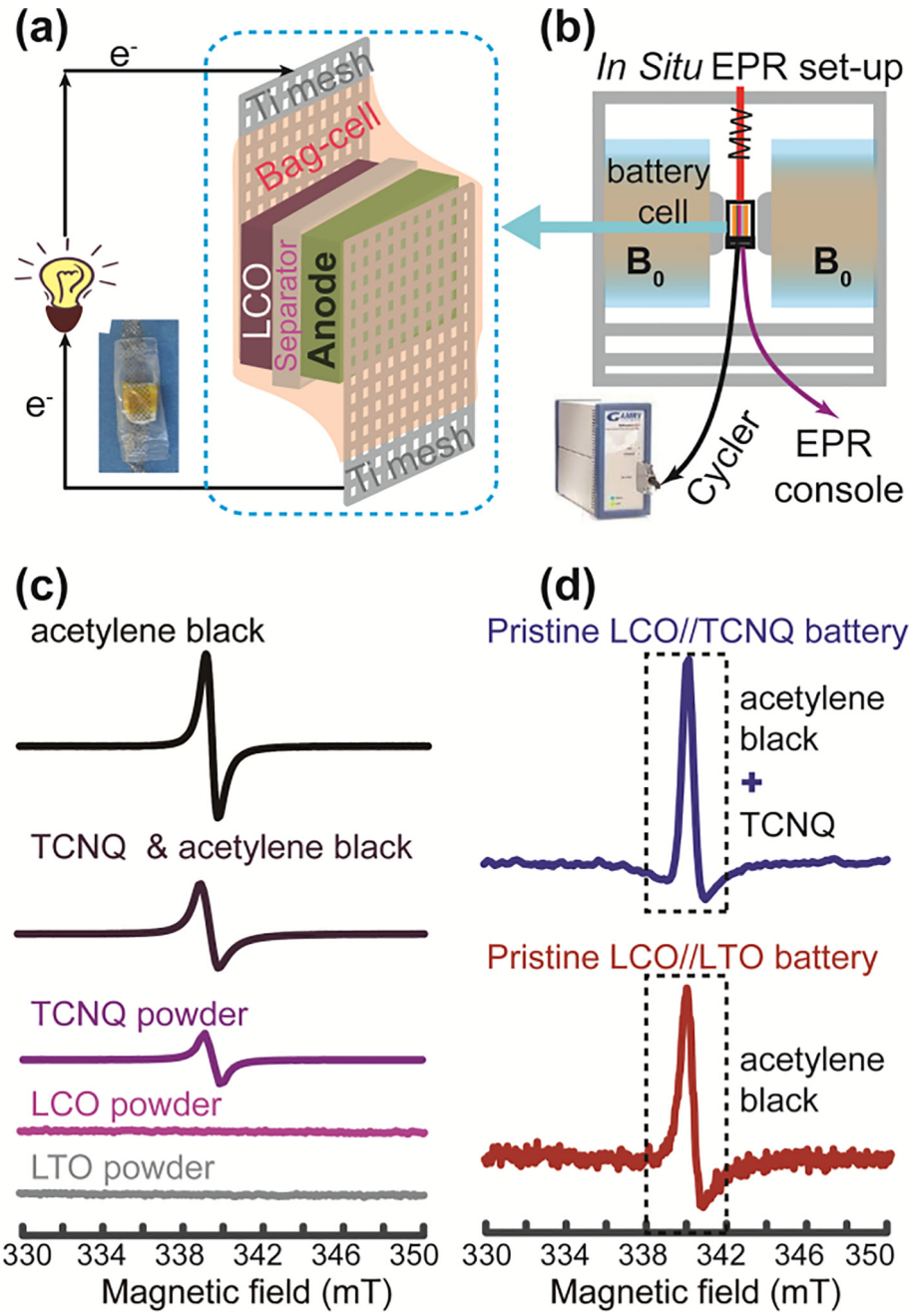

Fig. 1. The experimental setup for the *in situ* EPR acquisition and the EPR spectra from control experiments performed on battery components. (a) Schematic of a bag-cell battery for *in situ* EPR characterization positioned in the EPR cavity in a magnet as shown in (b). The battery is connected to a Gamry potentiostat and the EPR console for simultaneous acquisition of electrochemical profiles and EPR spectra. (c) EPR spectra of the components used within the batteries. (d) EPR spectra of an LCO//TCNQ and an LCO//LTO bag-cell battery acquired right after assembly.

of TCNQ [6], while others based on computational studies proposed TCNQ dimer formation [21,22]. However, no direct experimental evidence has been made available to either argument.

Various techniques, such as Infrared, Ramman, UV–vis, Nuclear Magnetic Resonance (NMR), and Scanning Transmission Electron Spectroscopy (STEM) have been explored to determine the structure and working mechanism of organic electrodes [9,12,15,17,18,23]. In particular, electron paramagnetic resonance (EPR), which is a sensitive technique for probing unpaired, conductive, and delocalized electrons, has been proved as a non-destructive and powerful tool for both *ex situ* [24–33] and *in situ* investigations of changes in electron states [34–41]. In this contribution, *in situ* EPR is employed to determine the states and distribution of electrons in TCNQ electrodes upon lithiation and delithiation. The gained new knowledge sheds light on the working mechanism of TCNQ electrodes and other quinone-based organic materials in rechargeable Li-ion batteries and provides insights into structural design for improved electrochemical performance of organic electrodes.

2. Experimental

2.1. Materials

7,7,8,8-tetracyanoquinodimethane (TCNQ), lithium cobalt oxide ($LiCoO_2$, 98%), and lithium titanate spinel oxide ($Li_4Ti_5O_{12}$, particle size < 100 nm) were purchased from Sigma Aldrich. They were dried at 120 ℃ for two days prior to making electrodes. Binder

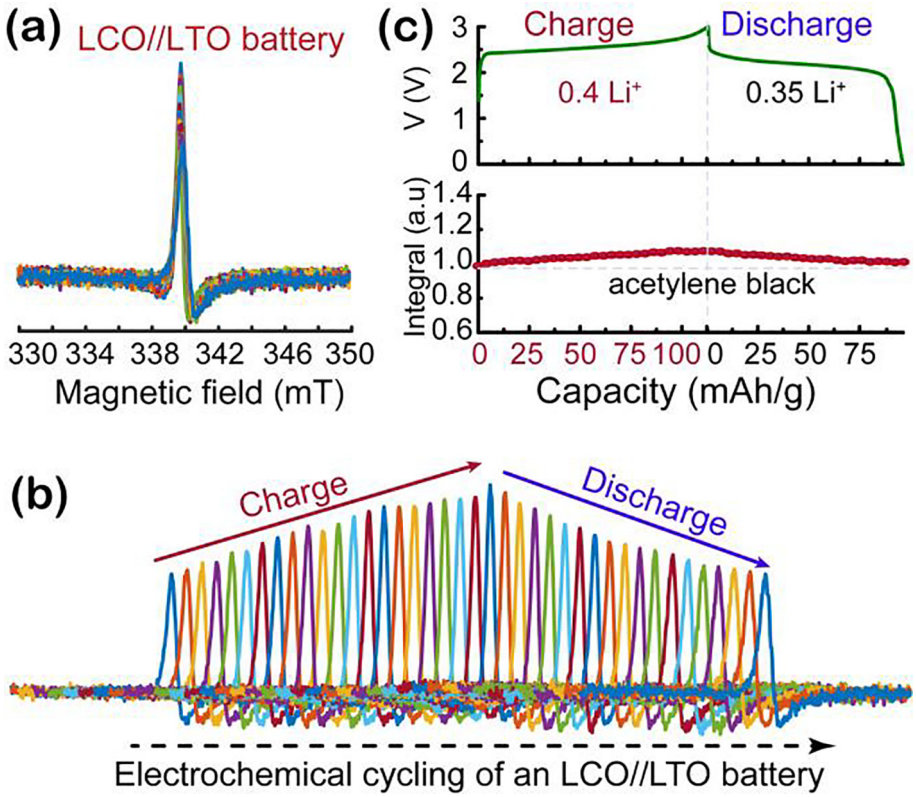

Fig. 2. *In situ* EPR spectra of an LCO//LTO bag-cell battery upon the 1st charge/discharge electrochemical cycling. (a) Overlapped and (b) sequentially displayed *in situ* EPR spectra for the first cycle and (c) the electrochemical profile and EPR spectral areal integrals of the LCO//LTO bag-cell battery as a function of charge states.

polyvinylidene fluoride (PVDF, Kynar Flex 2801, Arkema) and 60 wt% solution of polytetrafluoroethylene (PTFE, batch number #0011601, MTI Corporation) were used as received without further purification.

2.2. Sample preparation and characterization

2.2.1. Electrochemistry

The inorganic electrodes were made by mixing $LiCoO_2$ (LCO) and $Li_4Ti_5O_{12}$ (LTO) with polyvinylidene fluoride (PVDF) and conductive acetylene black (80:10:10, w:w:w). The mixture was dispersed in N-Methyl-2-pyrrolidone (NMP) and manually ground in an agate mortar for 30 minutes to form a homogenous slurry. The slurry was cast onto a Ti mesh and dried at 120 °C for 4 h under vacuum before assembled into batteries inside an Argon-filled glove-box.

A similar procedure was employed to make organic TCNQ electrodes. The active material TCNQ, binder PTFE, and acetylene black were mixed with a weight ratio of 60:10:30. Ethanol was used as the paste solvent during mixing in order to improve the contact between TCNQ and acetylene. The film obtained after ethanol evaporation was cut into small pieces, pressed onto Ti mesh, and dried under vacuum at 90 °C for 2 h. The obtained electrodes were transferred into an Argon-filled glove-box for battery assembly. The LCO cathode and LTO or TCNQ anode were separated by a piece of porous glass microfiber (Whatman, type GF/D), which was soaked in the LP30 electrolyte, *i.e.,* 1 M $LiPF_6$ in ethylene carbonate and dimethyl carbonate (1:1, w:w, Merck).

It is worth noting that different binders and conductive additive amount were used for LCO/LTO and LCO/TCNQ based on their electronic conductivities and physical properties, which was necessary to make the battery cells work. Nevertheless, the binders are EPR silent and examined with careful control experiments, and the EPR background is only originated from the evolution of acetylene black, which is carefully subtracted with our experiential design. Therefore, the difference in binder and ratio does not affect the data analysis and final conclusion.

For *in situ* EPR measurements, plastic bag cells were assembled in an Argon-filled glove-box and were electrochemically cycled inside an EPR cavity. The cell was cycled with a Gamry 600 + potentiostat. EPR spectra were collected while cycling the batteries at a rate of C/15, with the capacity of C = 130 and 260 $mAh{\cdot}g^{-1}$ for LCO and TCNQ, respectively.

2.2.2. EPR measurements

Continuous-wave EPR (CW-EPR) spectra were acquired on a Bruker Elexsys E680 spectrometer at X-band (9.5 GHz) (Bruker BioSpin, Billerica, MA), using a Bruker High Sensitivity cavity (ER 4119HS) equipped with a home-made holder to secure the battery. All spectra during battery cycling were recorded under the kinetics mode (the F2 dimension is set to time). Each spectrum was the average of 6 scans with a total scanning time of 18 minutes. An interval of 150 ms was set between the spectra. The recording window was set to 200 mT with 4096 data points, covering all the EPR resonances in the current study. The microwave power and modulation amplitude were set to 0.2 mW and 0.5 mT, respectively. The areal integrals of the recorded spectra were calculated using MATLAB and Easyspin [42]. The first data point was normalized to be 1.

3. Results and discussion

To investigate the lithiation and delithiation mechanism of TCNQ, a careful design of a full battery is necessary to avoid interference of EPR signals from other parts of the battery in addition to those originating from TCNQ. To prepare the battery cell, EPR

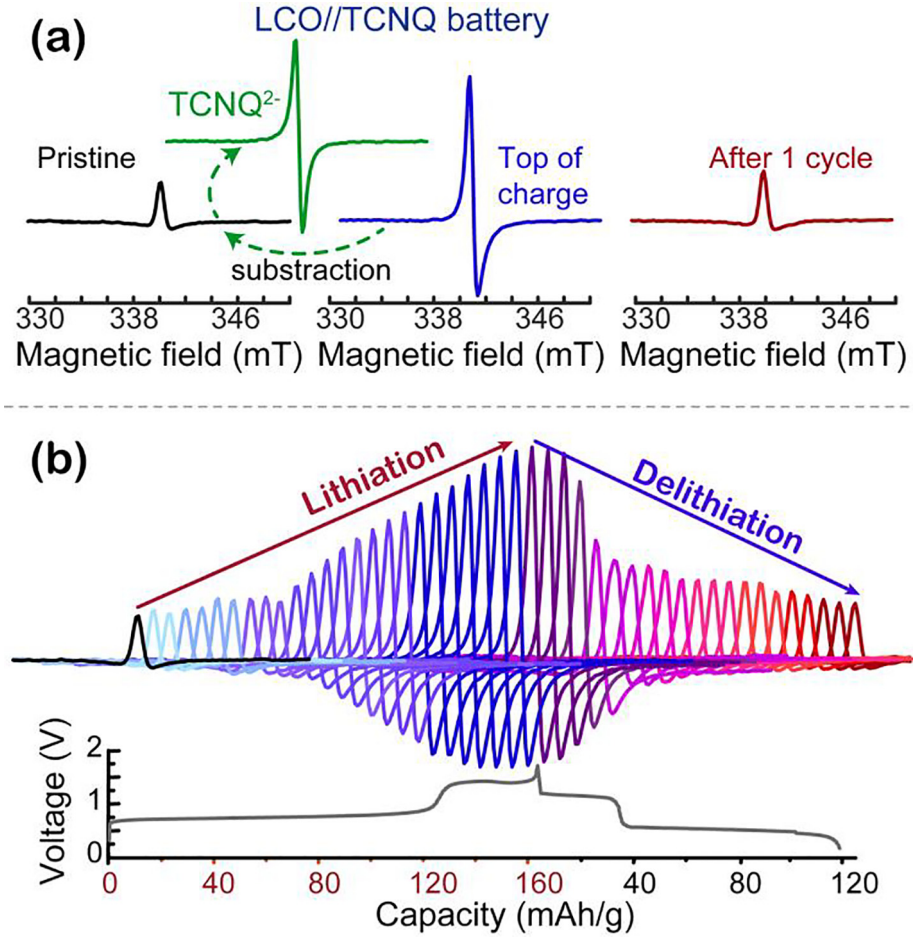

Fig. 3. *In situ* EPR of an LCO//TCNQ bag-cell battery upon electrochemical cycling. (a) EPR spectra of the freshly assembled battery at the top of charge and after one cycle, respectively. (b) All *in situ* EPR spectra for the first charge–discharge cycle, along with the corresponding electrochemical profile.

experiments are first performed on candidate active electrode materials and supporting components. Microwave penetration is often limited by metallic components of battery cells; therefore, bag-cell batteries are fabricated with Ti mesh as current collectors to maximize microwave (MW) penetration and *in situ* EPR sensitivity. Preparatory experiments have shown that the separator (glass fiber), air-tight plastic cover for the bag-cells, and Ti current collectors are EPR silent at room temperature. For *in situ* EPR acquisitions, the assembled bag-cell battery (Fig. 1a) is vertically positioned in the EPR cavity (Fig. 1b) and connected to a Gamry potentiostat for electrochemical operation. Control EPR experiments are first carried out on individual components (Fig. 1c) used in the batteries. Conductive acetylene black shows relatively intense EPR signals. Pristine TCNQ displays a weak EPR resonance due to delocalized electrons within its core [43]. The EPR spectrum of the electrodes containing a mixture of TCNQ, poly tetra fluoroethylene (PTFE), and acetylene black with a weight ratio of 6: 1: 3, is also acquired and shown in Fig. 1c (second spectrum from the top). Since the EPR resonances of TCNQ and Li metal overlap with each other, to avoid interference for quantitative analysis of EPR for TCNQ, EPR-silent LCO is chosen as the counter electrode. Both pristine LCO and LTO are EPR silent at room temperature at X-band as shown at the bottom of Fig. 1c, most likely due to large zero-field splitting and fast relaxation [44]. In fact, Ti^{3+} is EPR active and weak signals could be detected if the measured sample is under dry conditions. In this *in situ* study, the EPR signal from Ti^{3+} is negligible. Therefore, an LCO//LTO full battery is employed to determine the EPR signal evolution of acetylene black upon cycling, which will later be used for background correction to obtain the EPR signal purely from TCNQ. Thus, two sets of full batteries (LCO//LTO and LCO//TCNQ) are investigated. Both pristine LCO//TCNQ and LCO//LTO bag-cell batteries show asymmetric EPR spectra (Fig. 1d), which is possibly caused by organic carbonates coordinated to nearby Li^+ ions in the LP30 electrolyte [45–48], resembling the effect of the conductive bulk metals [34,39,36,49,50]. The EPR signal of the LCO//TCNQ battery originates from both acetylene black and TCNQ; the EPR signal of the LCO//LTO battery is from acetylene alone.

In order to evaluate the contribution to the EPR signal by acetylene black used as the conductive additive in the battery, the real-time evolution of the EPR signal from acetylene black is acquired on an LCO//LTO battery. *In situ* EPR spectra of the LCO//LTO battery during the 1st charge–discharge are shown in Fig. 2a and 2b. The EPR spectra exhibit the same line shape with intensity gradually increases upon charge and decreases upon discharge. The normalized spectral areal integral is plotted as a function of capacity shown in Fig. 2c, along with the electrochemical profile of the LCO//LTO battery cycled at a rate of C/15 with C = 137 mAh/g calculated based on the theoretical capacity of LCO by removing 0.5 Li per formula. Upon charge, about 0.4 Li is extracted from LCO and intercalated into LTO; upon discharge, 0.35 Li is deintercalated from LTO and reinserted back into LCO. The EPR signal intensity

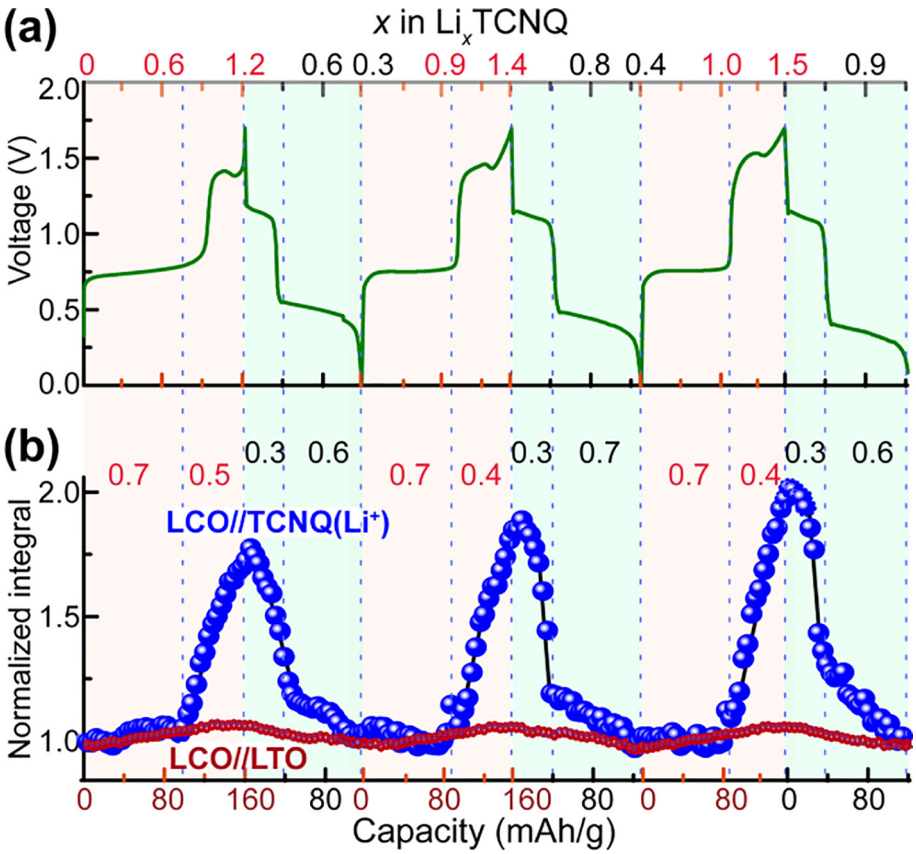

Fig. 4. Quantitative analysis of the *in situ* EPR on an LCO//TCNQ battery. (a) The electrochemical profile of the LCO//TCNQ battery during *in situ* EPR acquisition. (b) Normalized EPR spectral areal integral as a function of the specific capacity for the LCO//TCNQ battery. The areal integral of the EPR signal from the pristine battery is normalized to be 1. For reference, the spectral areal integral of EPR signal originating from components in the battery other than TCNQ is shown as dark brown dots, determined based on the *in situ* EPR control experiments on an LCO/LTO battery (Fig. 2).

of acetylene black is increased by about 10% at the top of charge compared with the pristine state, which is probably attributed to the redistribution of conductive electrons during the charge process. This change is almost recovered upon discharge. The EPR evolution of acetylene black used in these batteries will be taken into account for the following quantitative studies.

To help elucidate the working mechanism of TCNQ electrodes in rechargeable Li-ion batteries, *in situ* EPR experiments are performed on a bag-cell battery made of LCO//TCNQ. Since LCO is EPR silent at room temperature, it is used as the counter electrode to TCNQ and provides the necessary Li^+ source. The pristine LCO//TCNQ battery shows an asymmetric EPR resonance (Fig. 3a) mainly originating from the conductive additive acetylene black. The signal from pristine TCNQ contributes a very small fraction to the overall EPR resonance of the full battery, suggested by the results from the control experiments shown in Fig. 1c. However, at the top of charge (lithiated TCNQ), both positive and negative magnitudes grow significantly (spectrum in blue in Fig. 3b). The subtraction of the spectrum of the pristine battery from that of the top lithiated TCNQ gives rise to the change in EPR signal due to the lithiation process. The difference spectrum is plotted in green and labeled with $TCNQ^{2-}$ at the top of charge, as theoretically it will form a structure with the composition of Li_2TCNQ. The difference spectrum exhibits a symmetric shape, comparable to the ones from control experiments on electrolyte-free samples (Fig. 1c). At the end of the first charge–discharge cycle, the EPR spectrum is nearly recovered to the one acquired on the pristine battery (spectrum in red in Fig. 3a). The whole series of *in situ* EPR spectra following the first charge–discharge cycle is plotted in Fig. 3b, along with the corresponding electrochemical profiles shown below. Only slight increase in the EPR signal intensity of the LCO//TCNQ battery is observed at the beginning of lithiation of TCNQ, till reaching a capacity of 80 mAh/g. The growth of the EPR signal is significantly faster for the rest of the charging (lithiation) process. The reverse pattern of signal change is observed upon delithiation of TCNQ. The evolution of the *in situ* EPR signal reflects changes in redox reactions of TCNQ. Further quantitative analysis of these changes will afford more in-depth insights into the working mechanism of TCNQ electrodes *in situ*.

Quantitative analysis of changes in the EPR signal intensity of an LCO//TCNQ battery cell over the first three lithiation-delithiation cycles is performed and the results are summarized in Fig. 4b, along with the corresponding electrochemical profile of the LCO//TCNQ bag-cell battery shown in Fig. 4a. About 0.9 Li is intercalated into TCNQ during the 1st plateau at 0.75 V and 0.3 Li for the 2nd plateau at 1.4 V. The obtained capacities are lower than the theoretical value, *i.e.*, 1 Li for each plateau, which is attributed to a few reasons: i) inadequate amount of electrolyte is used in the batteries, since $-CH_3$ group within the solvents of LP30 electrolytes greatly affects EPR cavity tuning and poor tuning results in significantly reduced detection sensitivity; ii) dissolution of TCNQ in the electrolyte; iii) low electronic conductivity of the TCNQ electrode, yielding a fraction of TCNQ in the electrode not accessible. All these factors will lead to capacity reduction, which will be considered in the following analysis. Upon discharge, 0.3 Li is extracted from TCNQ over the first plateau at 1.15 V and 0.6 Li during the 2nd plateau at about 0.5 V. A hysteresis of 0.25 V is observed for both plateaus during the lithiation process of TCNQ.

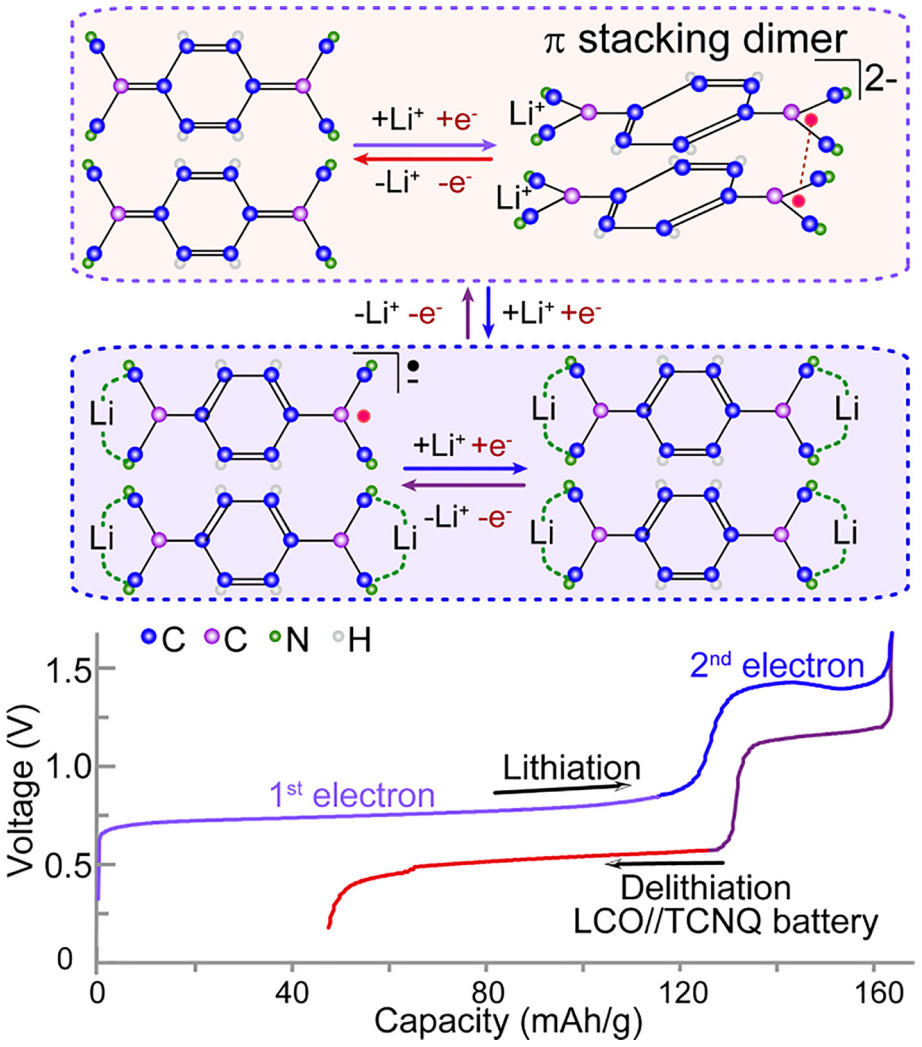

Fig. 5. Proposed mechanism for (de)lithiation of TCNQ within an LCO//TCNQ battery, based on this *in situ* EPR study.

These patterns are observed beyond the first cycle with the same cycling rate of C/15 (Fig. 4a). Upon further charge, about 0.7 Li at the lower plateau and 0.4 Li at the higher plateau are intercalated into TCNQ. 0.3 Li at the higher plateau and 0.7 Li at the lower plateau are extracted from TCNQ upon discharge. The irreversible capacity is possibly attributed to the low electronic conductivity of state of change TCNQ and insufficient electrolyte. 1.1 Li is further intercalated into TCNQ and 0.9 Li is extracted upon the 3rd charge and discharge. The 2nd plateau is shorter than the 1st one displayed in the three presented cycles is possibly due to the high resistance caused by insufficient electrolyte. Although full capacity is not achieved, the following analysis and results can sufficiently support the two-electron reaction mechanism.

Spectral areal integrals of the *in situ* EPR of the LCO//TCNQ battery mentioned above are plotted in Fig. 4b, together with those of an LCO//LTO battery for reference. The former set of integrals include contributions from TCNQ, acetylene black, and electrolyte, and the latter from acetylene black and electrolyte; therefore, the difference between these two sets of integrals reflects evolution of EPR signals purely from TCNQ in the electrode. As shown in Fig. 4b, at the initial lithiation of TCNQ up to 0.7 Li^+/TCNQ, no net change in the EPR resonance from TCNQ or lithiated-TCNQ is observed, suggesting that no radicals are formed or significant change in ERP-relevant electron properties. Near the end of the 1st plateau and during the entire 2nd plateau upon lithiation, the *in situ* EPR signal rapidly grows in almost a linear fashion, indicating continuous formation of TCNQ monomer radicals. The reversible process is observed upon delithiation. The same trend is observed but with increased maximum intensity for the next two lithiation-delithiation cycles. This is mainly due to increased intercalation of Li into TCNQ, which contains 1.2, 1.4, and 1.5 Li to total at top of charge during the three cycles. In addition, the disorder caused by cycling can possibly promote delocalization of electrons with enhanced EPR signal as well [24,26,28,51].

According to the above results and discussion, the reaction mechanism of lithiation and delithiation of TCNQ is proposed as shown in Fig. 5. During lithiation, Li^+ inserts between two cyanide groups in TCNQ, consistent with previous computational studies [22,52]. Meanwhile, e^- imparts into TCNQ, resulting in electron re-distribution (or chemical bond re-configuration) within the entire molecule and transforming a quinone ring into a benzene ring. The unpaired electron within each lithiated-TCNQ molecule promotes its coupling to another lithiated-TCNQ, forming a pi-stacking dimer. This explains the reason why early-stage lithiation of TCNQ does not yield net EPR signal gain. Upon further lithiation, the inserted Li^+ ions break down the previously formed dimers, yielding Li^+-$TCNO^-$, which allows further delocalization of electrons within the entire molecule, resulting in increased EPR signal. Upon delithiation, a reversible process occurs, including the dimer formation at the intermediate stage after removal of one Li^+ and e^-.

This mechanism including TCNQ dimer formation is also supported by our NMR results in a separate study.

4. Conclusions

In situ EPR has been performed on the lithiation and delithiation process of organic TCNQ electrodes. The integrated EPR signal reveals no evidence of radical formation during the early stage of lithiation, instead, TCNQ dimers are formed during the first electron and lithium insertion. The 2nd electron and lithium insertion breaks down the dimers and allows sufficient delocalization of electrons within the formed benzene anions, which leads to the observed increase in EPR signal. The TCNQ core is perturbed upon further cycling, confirmed by the increased maximum EPR signal at the end of each lithiation-delithiation cycle. *In situ* EPR serves as a powerful, sensitive, and convenient tool to follow electron activities, which in turn affords insights into reaction mechanisms of organic electrodes in rechargeable batteries in real-time.

Declaration of Competing Interest

The authors declare that they have no known competing financial interests or personal relationships that could have appeared to influence the work reported in this paper.

Acknowledgments

This work was supported by the National Science Foundation under Grant No. DMR-1847038. All EPR experiments were carried out at the NHMFL which is supported by the National Science Foundation Cooperative Agreement No. DMR-1644779 and the State of Florida.

References

[1] J.-M. Tarascon, M. Armand, Nature 414 (2001) 359–367.
[2] M. Armand, J.-M. Tarascon, Nature 451 (2008) 652–657.
[3] Y. Wen, X. Chen, X. Lu, L. Gu, J. Energy Chem. 27 (2018) 1397–1401.
[4] N. Zhang, X. Zhang, E. Shi, S. Zhao, K. Jiang, D. Wang, P. Wang, S. Guo, P. He, H. Zhou, J. Energy Chem. 27 (2018) 1655–1660.
[5] Y. Chen, Y. Kang, Y. Zhao, L. Wang, J. Liu, Y. Li, Z. Liang, X. He, X. Li, N. Tavajohi, B. Li, J. Energy Chem. (2020) doi.org/10.1016/j.jechem.2020.10.017
[6] Y. Hanyu, I. Honma, Sci. Rep. 2 (2012) 453–458.
[7] Y. Liang, Y. Jing, S. Gheytani, K.-Y. Lee, P. Liu, A. Facchetti, Y. Yao, Nat. Mater. 16 (2017) 841–848.
[8] Y. Lu, Q. Zhang, L. Li, Z. Niu, J. Chen, Chemistry 4 (2018) 2786–2813.
[9] Z. Song, Y. Qian, X. Liu, T. Zhang, Y. Zhu, H. Yu, M. Otani, H. Zhou, Energy Environ. Sci. 7 (2014) 4077–4086.
[10] X. Chi, Y. Liang, F. Hao, Y. Zhang, J. Whiteley, H. Dong, P. Hu, S. Lee, Y. Yao, Angew. Chem. Int. Ed. 57 (2018) 2630–2634.
[11] W. Huang, Z. Zhu, L. Wang, S. Wang, H. Li, Z. Tao, J. Shi, L. Guan, J. Chen, Angew. Chem. Int. Ed. 52 (2013) 9162–9166.
[12] W. Huang, S. Zheng, X. Zhang, W. Zhou, W. Xiong, J. Chen, Energy Storage Mater. 26 (2020) 465–471.
[13] K. Taniguchi, K. Narushima, J. Mahin, W. Kosaka, H. Miyasaka, Angew. Chem. Int. Ed. 55 (2016) 5238–5242.
[14] C. Fang, Y. Huang, L. Yuan, Y. Liu, W. Chen, Y. Huang, K. Chen, J. Han, Q. Liu, Y. Huang, Angew. Chem. Int. Ed. 56 (2017) 6793–6797.
[15] W. Xiong, W. Huang, M. Zhang, P. Hu, H. Cui, Q. Zhang, Chem. Mater. 31 (2019) 8069–8075.
[16] T.B. Schon, B.T. McAllister, P.-F. Li, D.S. Seferos, Chem. Soci. Rev. 45 (2016) 6345–6404.
[17] B. Häupler, R. Burges, T. Janoschka, T. Jähnert, A. Wild, U.S. Schubert, J. Mater. Chem., A 2 (2014) 8999–9001.
[18] J. Xie, Q. Zhang, J. Mater. Chem. A 4 (2016) 7091–7106.
[19] M. Miroshnikov, K.P. Divya, G. Babu, M. Meiyazhagan, L.M.R. Arava, P.M. Ajayan, G. John, J. Mater. Chem., A 4 (2016) 12370–12386.
[20] C. Han, H. Li, R. Shi, T. Zhang, J. Tong, J. Li, B. Li, J. Mater. Chem., A 7 (2019) 23378–23415.
[21] M.C. Grossel, F.A. Evans, J.A. Hriljac, K. Prout, S.C. Weston, J. Chem. Soc., Chem. Commun. 1 (1990) 1494–1495.
[22] Z.-J. Li, Z.-R. Li, F.-F. Wang, F. Ma, M.-M. Chen, X.-R. Huang, Chem. Phys. Lett. 468 (2009) 319–324.
[23] Y. Jing, Y. Liang, S. Gheytani, Y. Yao, Nano Energy 37 (2017) 46–52.
[24] B. Grossmann, J. Heinze, T. Moll, C. Palivan, S. Ivan, G. Gescheidt, J. Phys. Chem. B 108 (2004) 4669–4672.
[25] C.E. Tait, P. Neuhaus, M.D. Peeks, H.L. Anderson, C.R. Timmel, J. Am. Chem. Soc. 137 (2015) 8284–8293.
[26] J. Rawson, P.J. Angiolillo, M.J. Therien, P. Natl. Acad. Sci. 112 (2015) 13779–13783.
[27] H. Kaftelen, M. Tuncer, S. Tu, S. Repp, H. Goçmez, R. Thomann, S. Weber, E. Erdem, J. Mater. Chem. 1 (2013) 9973–9982.
[28] M.D. Peeks, C.E. Tait, P. Neuhaus, G.M. Fischer, M. Hoffmann, R. Haver, A. Cnossen, J.R. Harmer, C.R. Timmel, H.L. Anderson, J. Am. Chem. Soc. 139 (2017) 10461–10471.
[29] C. Berthier, J.R. Cooper, D. Jerome, G. Soda, C. Weyl, J.M. Fabre, L. Giral, Mol. Cryst. Liq. Cryst. 32 (1976) 267–270.
[30] M. Botko, E. Čižmár, M. Kajňaková, A. Feher, Acta Phys. Pol., A 126 (2014) 252–253.
[31] S. Richert, C.E. Tait, C.R. Timmel, J. Magn. Res. 280 (2017) 103–116.
[32] C. Li, M. Shen, X. Lou, B. Hu, J. Phys. Chem. C 122 (2018) 27224–27232.
[33] S. Gu, S. Wu, L. Cao, M. Li, N. Qin, J. Zhu, Z. Wang, Y. Li, Z. Li, J. Chen, Z. Lu, J. Am. Chem. Soc. 141 (2019) 9623–9628.
[34] J. Wandt, C. Marino, H.A. Gasteiger, P. Jakes, R.-A. Eichel, J. Granwehr, Energy Environ. Sci. 8 (2015) 1358–1367.
[35] Q. Wang, J. Zheng, E. Walter, H. Pan, D. Lv, P. Zuo, H. Chen, Z.D. Deng, B.Y. Liaw, X. Yu, X. Yang, J.-G. Zhang, J. Liu, J. Xiao, J. Electrochem. Soc. 162 (2015) A474–A478.
[36] M. Sathiya, J.-B. Leriche, E. Salager, D. Gourier, J.-M. Tarascon, H. Vezin, Nat. Commun. 6 (2015) 6276.
[37] J.B. Priebe, M. Karnahl, H. Junge, M. Beller, D. Hollmann, A. Brückner, Angew. Chem. Int. Ed. 5 (2013) 11420–11424.
[38] J. Rabeah, U. Bentrup, R. Stçßer, A. Brückner, Angew. Chem. Int. Ed. 54 (2015) 11791–11794.
[39] J. Wandt, P. Jakes, J. Granwehr, R.-A. Eichel, H.A. Gasteiger, Mater. Today 21 (2017) 231–240.
[40] M. Tang, A. Dalzini, X. Li, X. Feng, P.-H. Chien, L. Song, Y.-Y. Hu, J. Phys. Chem. Lett. (2017) 4009–4016.
[41] J. Wang, M. Yang, C. Zhao, B. Hu, X. Lou, F. Geng, W. Tong, B. Hu, C. Li, Phys. Chem. Chem. Phys. 21 (2019) 24017–24025.
[42] S. Stoll, A. Schweiger, J. Magn. Reson. 178 (2006) 42–55.
[43] A. Ishitani, S. Nagakura, Mol. Phys. 12 (1967) 1–12.
[44] J. Krzystek, A. Ozarowski, J. Telser, Coord. Chem. Rev. 250 (2006) 2308–2324.
[45] A.L. Michan, M. Leskes, C.P. Grey, Chem. Mater. 28 (2016) 385–398.
[46] Y. Jin, N.-J.-H. Kneusels, P.C.M.M. Magusin, G. Kim, E. Castillo-Martínez, L.E. Marbella, R.N. Kerber, D.J. Howe, S. Paul, T. Liu, C.P. Grey, J. Am. Chem. Soc. 139 (2017) 14992–15004.
[47] N.M. Trease, L. Zhou, H.J. Chang, B.Y. Zhu, C.P. Grey, Solid State Nucl. Magn. Reson. 42 (2012) 62–70.
[48] L. Zhou, M. Leskes, A.J. Ilott, N.M. Trease, C.P. Grey, J. Magn. Reson. 234 (2013) 44–57.
[49] F.J. Dyson, Phys. Rev. 98 (1955) 349–359.
[50] G. Feher, A.F. Kip, Phys. Rev. 98 (1955) 337–348.
[51] A.L. Sutton, B.F. Abrahams, D.M. D'Alessandro, T.A. Hudson, R. Robson, P.M. Usov, Cryst. Eng. Comm. 18 (2016) 8906–8914.
[52] Y. Chen, S. Manzhos, Phys. Chem. Chem. Phys. 18 (2016) 1470–1477.